Low-Velocity-Favored Transition Radiation

Jialin Chen,[1,2,3] Ruoxi Chen,[1,2] Fuyang Tay,[4,5] Zheng Gong,[1,2] Hao Hu,[6] Yi Yang,[7] Xinyan Zhang,[1,2] Chan Wang,[1,2,8] Ido Kaminer,[3,*] Hongsheng Chen,[1,2,8,9,†] Baile Zhang,[10,11] and Xiao Lin[1,2,‡]

[1]*Interdisciplinary Center for Quantum Information, State Key Laboratory of Extreme Photonics and Instrumentation, ZJU-Hangzhou Global Scientific and Technological Innovation Center, College of Information Science & Electronic Engineering, Zhejiang University, Hangzhou 310027, China*

[2]*International Joint Innovation Center, the Electromagnetics Academy at Zhejiang University, Zhejiang University, Haining 314400, China*

[3]*Department of Electrical and Computer Engineering, Technion-Israel Institute of Technology, Haifa 32000, Israel*

[4]*Department of Electrical and Computer Engineering, Rice University, Houston, Texas 77005, USA*

[5]*Applied Physics Graduate Program, Smalley-Curl Institute, Rice University, Houston, Texas 77005, USA*

[6]*School of Electrical and Electronic Engineering, Nanyang Technological University, Singapore 639798, Singapore*

[7]*Department of Physics, University of Hong Kong, Hong Kong 999077, China*

[8]*Key Lab of Advanced Micro/Nano Electronic Devices & Smart Systems of Zhejiang, Jinhua Institute of Zhejiang University, Zhejiang University, Jinhua 321099, China*

[9]*Shaoxing Institute of Zhejiang University, Zhejiang University, Shaoxing 312000, China*

[10]*Division of Physics and Applied Physics, School of Physical and Mathematical Sciences, Nanyang Technological University, Singapore 637371, Singapore*

[11]*Centre for Disruptive Photonic Technologies, Nanyang Technological University, Singapore 637371, Singapore*

(Received 29 November 2022; accepted 10 August 2023; published 13 September 2023)

When a charged particle penetrates through an optical interface, photon emissions emerge—a phenomenon known as transition radiation. Being paramount to fundamental physics, transition radiation has enabled many applications from high-energy particle identification to novel light sources. A rule of thumb in transition radiation is that the radiation intensity generally decreases with the decrease of particle velocity v; as a result, low-energy particles are not favored in practice. Here, we find that there exist situations where transition radiation from particles with extremely low velocities (e.g., $v/c < 10^{-3}$) exhibits comparable intensity as that from high-energy particles (e.g., $v/c = 0.999$), where c is the light speed in free space. The comparable radiation intensity implies an extremely high photon extraction efficiency from low-energy particles, up to 8 orders of magnitude larger than that from high-energy particles. This exotic phenomenon of low-velocity-favored transition radiation originates from the interference of the excited Ferrell-Berreman modes in an ultrathin epsilon-near-zero slab. Our findings may provide a promising route toward the design of integrated light sources based on low-energy electrons and specialized detectors for beyond-standard-model particles.

DOI: 10.1103/PhysRevLett.131.113002

Transition radiation occurs whenever a charged particle moves across an inhomogeneous region [1–8]; as shown in Fig. 1. One unique feature of transition radiation is that its radiation intensity is linearly proportional to the Lorentz factor $\gamma = (1 - v^2/c^2)^{-1/2}$ [9], if the particle velocity v approaches the light speed c in free space. This feature lays the foundation for many applications, including transition radiation detectors [10–12], useful for the identification of particles with extremely high momenta (e.g., $P > 100$ GeV$/c$ or $\gamma > 10^5$) [9], as well as advanced light sources at the terahertz, ultraviolet, and x-ray regimes [13–21]. However, all these transition-radiation-based devices rely on high-energy particles, whose generation requires a giant and complex acceleration infrastructure and thus hinders the enticing on-chip applications of transition radiation.

Another feature of transition radiation is that its occurrence has no specific requirements on the particle velocity [1–8]. This feature is distinct from Cherenkov radiation [22–27], which occurs when a charged particle moves inside a homogeneous material with a velocity exceeding the phase velocity of light, namely the Cherenkov threshold [28–32]. As such, all applications of Cherenkov radiation are limited by the Cherenkov threshold, despite its enormous applications [33–39], including particle detectors, light sources, imaging, and photodynamic therapy. By contrast, transition radiation is applicable to develop novel light sources without fundamental restrictions on the particle velocities. However, the application of transition radiation based on low-energy particles remains largely unexplored. One reason is that the transition-radiation intensity generally decreases when the particle velocity

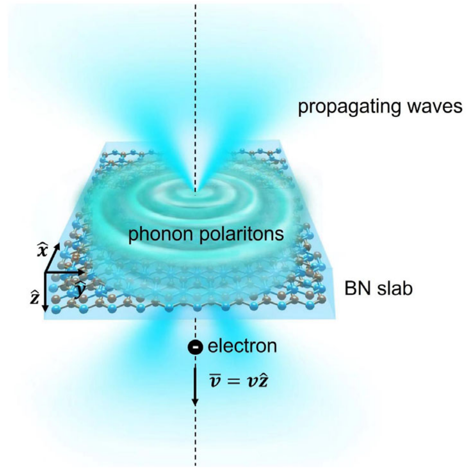

FIG. 1. Schematic of low-velocity-favored transition radiation from a uniaxial epsilon-near-zero (ENZ) material. A swift electron perpendicularly penetrates through a BN slab with a relative permittivity of $[\varepsilon_\perp, \varepsilon_\perp, \varepsilon_z]$, where $|\varepsilon_z| \to 0$ near 24.5 THz. Unless specified otherwise, the material loss is considered in this work. Both the propagating waves and phonon polaritons would be excited during the electron's penetration. Below, we focus on the light emission propagating into the far field, which is irrelevant to the excited phonon polaritons.

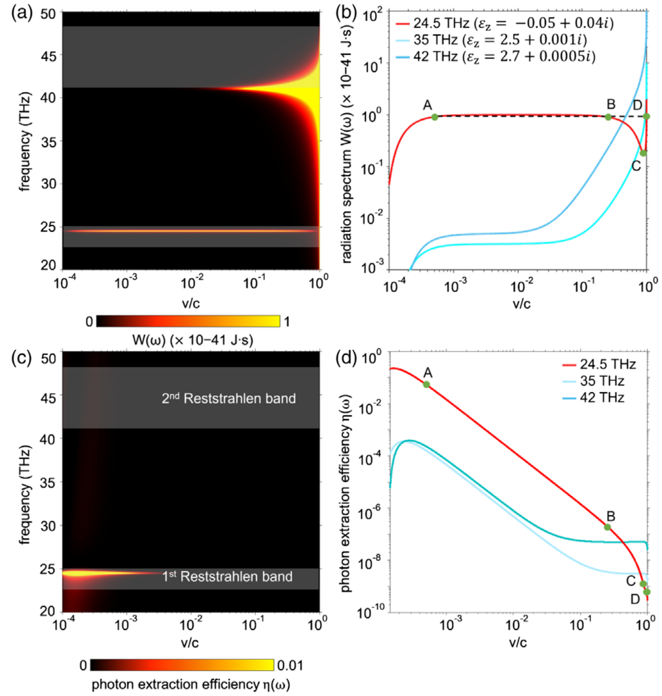

FIG. 2. Frequency spectral feature of low-velocity-favored transition radiation. (a) Radiation spectrum $W(\omega)$ of the excited propagating waves as a function of the electron velocity v and the frequency. (b) Radiation spectrum as a function of v at three representative frequencies. Here and below, when $\omega/2\pi = 24.5$ THz, the value of $W(\omega)$ at $v = v_A$ or $v = v_B$ is defined to be 90% of the maximum within the range of $v \in [v_A, v_B]$. (c),(d) Photon extraction efficiency $\eta(\omega) = W(\omega)/(\hbar\omega \cdot E_k)$, where E_k is the kinetic energy.

decreases. For example, the intensity of conventional transition radiation from low-energy particles with $v/c = 0.1$ can be 2 orders of magnitude weaker than that from high-energy particles with $v/c = 0.9$, as exemplified in Fig. 2. The enhancement of transition radiation from low-energy particles remains an open challenge in science and technology.

Here, we reveal a feasible route to enhance transition radiation from low-energy particles (e.g., free electrons) by exploiting the Ferrell-Berreman mode, which was first identified by Ferrell in 1958 in metal films at the ultraviolet regime [40] and later separately discussed by Berreman in 1963 in cubic ionic films at the midinfrared regime [41]. This mode is intrinsically radiative and appears near the frequency at which the relative permittivity of materials approaches zero. Moreover, the Ferrell-Berreman mode has enabled many applications [42–45] from imaging, sensing, to thin-film characterization. The transition radiation of Ferrell-Berreman modes has also been extensively studied since 1958 [4,46–49]. However, among these studies, the intensity dependence of the emitted Ferrell-Berreman mode on the particle velocity has been rarely discussed so far. Moreover, whether the Ferrell-Berreman mode can largely enhance the transition radiation from low-energy particles remains unknown.

Here, we find that due to the excitation of Ferrell-Berreman modes, low-energy particles with an extremely low velocity (e.g., $v/c < 10^{-3}$) could emit equally strong transition radiation as high-energy particles ($v/c = 0.999$). Consequently, the photon extraction efficiency from low-energy particles could be 8 orders of magnitude larger than that from high-energy particles, while the intensity of transition radiation from these particles is the same. This exotic phenomenon of free-electron radiation is then denoted as low-velocity-favored transition radiation, which is in a similar rationale but fundamentally different from low-velocity-favored Smith-Purcell radiation [50]. The revealed low-velocity-favored transition radiation indicates a promising route to enhance the particle-matter interaction, which may be exploited to design specialized detectors for beyond-standard-model particles with extremely low kinetic energy (e.g., detection of unknown millicharged dark matter [51–53]) and integrated light sources from low-energy electrons.

We begin with the introduction of transition radiation; see derivation in Supplemental Material, Sec. S1 [54]. An electron moves along the $+\hat{z}$ direction and perpendicularly penetrates through a thin epsilon-near-zero slab with a thickness d [Fig. 1]. The epsilon-near-zero slab (namely, region 2), for example, is constructed by hexagonal boron nitride (BN) [55–61] with a relative permittivity of $[\varepsilon_\perp, \varepsilon_\perp, \varepsilon_z]$, which has $\varepsilon_z \to 0$ around 24.5 THz. Both the superstrate (region 1) and the substrate (region 3) are free space with a relative permittivity of $\varepsilon_1 = \varepsilon_3 = 1$.

Within the framework of macroscopic Maxwell equations, the induced radiation fields in regions 1 and 3 can be calculated, and the total angular spectral energy density of transition radiation is obtained as $U(\omega,\theta) = U_1(\omega,\theta) + U_3(\omega,\theta)$, where θ is the radiation angle between the wave vector of excited propagating waves and $-\hat{z}$ $(+\hat{z})$ for the backward (forward) radiation. $U_1(\omega,\theta)$ and $U_3(\omega,\theta)$ are the angular spectral energy densities of backward and forward radiation, respectively, whose calculation includes the light emission from the interface and that from the bulk. Accordingly, the total energy spectrum can be expressed as $W(\omega) = \int_0^{\pi/2} U(\omega,\theta)(2\pi\sin\theta)\,d\theta$. The detailed calculation of angular spectral energy densities and energy spectra of excited propagating waves is provided in Supplemental Material, Sec. S2, and their calculation is not related to the excited guided modes (e.g., BN's phonon polaritons [55–58]) and is thus not necessary to apply the Sommerfeld integration [3,5,62–64].

As shown in Fig. 2(a), $W(\omega)$ is not only a function of the particle velocity but also sensitive to the frequency, due to the dispersive nature of BN. The BN thickness is 1 nm; see the influence of thickness on low-velocity favored transition radiation in Fig. S7. One may drill a hole at the slab along the electron trajectory to avoid the potential scattering of swift electrons; the hole diameter should be small enough, for example, around the scale of $v\lambda/(2\pi c)$, in order to enable sufficient interaction between the BN slab and the evanescent waves carried by swift electrons, where λ is the working wavelength of light in free space; see Supplemental Material, Sec. S10 [54]. Figure 2(a) shows that the frequency spectral feature of transition radiation near the frequency with $\varepsilon_z \to 0$ is different from the other frequency regimes. For better illustration, Fig. 2(b) shows $W(\omega)$ as a function of the electron velocity at three representative frequencies, namely 24.5 THz (within the first Reststrahlen band of BN) with $\varepsilon_\perp = 7.7 + 0.01i$ and $\varepsilon_z = -0.05 + 0.04i$, 42 THz (within the second Reststrahlen band) with $\varepsilon_\perp = -34.8 + 4.6i$ and $\varepsilon_z = 2.7 + 0.0005i$, and 35 THz (outside these two Reststrahlen bands) with $\varepsilon_\perp = 11.6 + 0.1i$ and $\varepsilon_z = 2.5 + 0.001i$. At 35 or 42 THz without $\varepsilon_z \to 0$, $W(\omega)$ monotonically increases with v in Fig. 2(b). By contrast, at $\omega_0/2\pi = 24.5$ THz with $\varepsilon_z \to 0$, $W(\omega_0)$ first increases with v if $v < v_A$, becomes insensitive to the variation of v if $v \in [v_A, v_B]$, then decreases with v if $v \in [v_B, v_C]$, and increases again with v if $v > v_C$, where $v_A = 4.5 \times 10^{-4}c$, $v_B = 2.6 \times 10^{-1}c$, and $v_C = 0.9c$. Remarkably, Fig. 2(b) also shows that the radiation intensity at the frequency with $\varepsilon_z \to 0$ can be 2 orders of magnitude larger than that at the frequency without $\varepsilon_z \to 0$ if $v/c < 10^{-1}$. Moreover, the values of $W(\omega_0)$ are the same, if the electron velocity is equal to v_A, v_B, or v_D, where $v_D = 0.999c$. For these velocities, the corresponding kinetic energy varies from $E_{k,A} = 51.7$ meV, $E_{k,B} = 18.2$ keV to $E_{k,D} = 10.9$ MeV. This exotic feature at 24.5 THz in Figs. 2(a) and 2(b) indicates that the transition radiation from low-energy particles can achieve the same radiation intensity as that from high-energy particles.

Upon close inspection, we find that the analytical limit of total energy spectrum $W(\omega)$ is essentially irrelevant to v, under the conditions of $\varepsilon_z(\omega) \to 0$, $\omega d/c \ll \sqrt{|\varepsilon_z/\varepsilon_\perp|}$, and $\omega d/c \ll v/c \ll 1$; see Supplemental Material, Sec. S5, as well as Figs. S2 and S3 [54]. Moreover, the limit of $W(\omega)$ is almost proportional to $1/|\varepsilon_z|^2$ in Fig. S3. This mathematically explains the emergence of low-velocity-favored transition radiation from an ultrathin epsilon-near-zero slab, which is featured with a plateau of largely enhanced radiation spectrum within the velocity range of $v \in [v_A, v_B]$ in Fig. 2(b). Since the condition of $\omega d/c \ll v/c \ll 1$ is dependent on d, this velocity range within which the low-velocity-favored transition radiation could occur is sensitive to d in Fig. S2.

According to Figs. 2(a) and 2(b), the photon extraction efficiency is further obtained as $\eta(\omega) = [W(\omega)/(\hbar\omega \cdot E_k)]$, where $E_k = m_e c^2(\gamma - 1)$ is the kinetic energy, m_e is the rest mass, and $\gamma = (1 - v^2/c^2)^{-1/2}$ is the Lorentz factor. Figure 2(c) shows the photon extraction efficiency as a function of frequency and velocity. From Fig. 2(c), if $v/c < 10^{-2}$, the maximum value of $\eta(\omega)$ always appears near the frequency with $\varepsilon_z \to 0$. Upon close inspection, Fig. 2(d) shows $\eta(\omega)$ as a function of velocity at three representative frequencies. When $v/c < 10^{-2}$, the photon extraction efficiency at 24.5 THz is nearly 3 orders of magnitude greater than those at 42 and 35 THz. Moreover, at $\omega_0/2\pi = 24.5$ THz, the value of $\eta(\omega_0)$ at point A with $v_A/c = 4.5 \times 10^{-4}$ is 8 orders of magnitude higher than that at point D with $v_D/c = 0.999$ in Fig. 2(d), although the values of $W(\omega_0)$ at these two points are the same in Fig. 2(b).

Besides the unique frequency spectral features in Fig. 2, this low-velocity-favored transition radiation also has exotic angular spectral features in Fig. 3. Figures 3(a)–3(d) illustrate the angular spectral energy density $U(\omega,\theta)$ as a function of velocity and radiation angle θ. At the frequency with $\varepsilon_z \to 0$, the dependence of $U(\omega,\theta)$ on v is not monotonical but rather complex in Figs. 3(a) and 3(b). Moreover, if the electron velocity is small (e.g., $v/c < 0.3$), the maximum of $U(\omega,\theta)$ still appears at a relatively large radiation angle (>80°) with a relatively large angular width (>50°) in Figs. 3(a) and 3(b). This feature for low-energy electrons is different from that for high-energy electrons. Generally, if $v \to c$ or $\gamma \gg 1$, the maximum of $U(\omega,\theta)$ would appear at $\theta \to 0°$ with a very narrow angular width (<0.1°) [9]. Since the resonance transition radiation is able to simultaneously improve the directivity and intensity of light emission [2], the relatively poor directivity of low-velocity-favored transition radiation might be overcome through the formation of resonance transition radiation by letting the moving electron interact with an epsilon-near-zero-material-based photonic crystal.

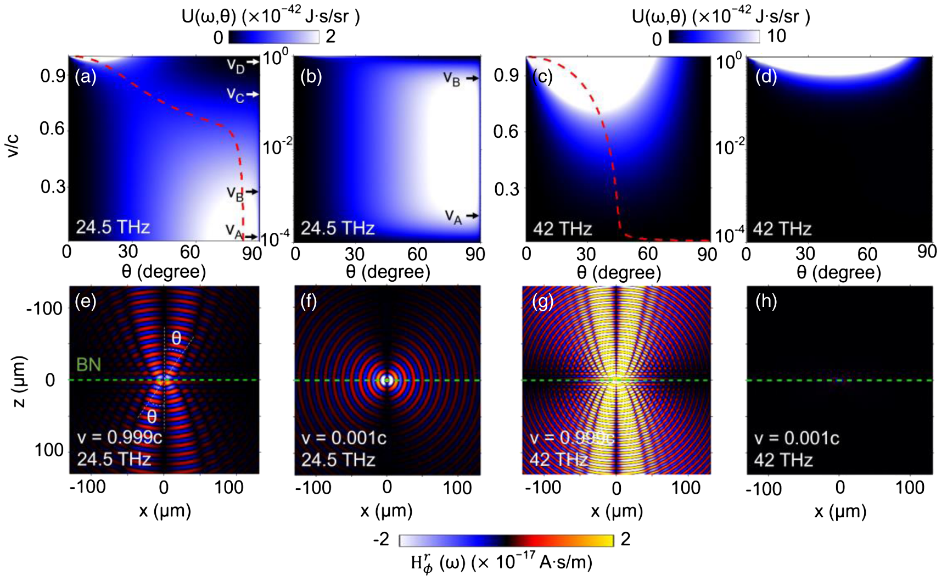

FIG. 3. Angular spectral feature of low-velocity-favored transition radiation. (a)–(d) Angular spectral energy density $U(\omega,\theta)$ of transition radiation as a function of the radiation angle θ and the electron velocity v. Each red dashed line indicates the angular trajectory of the maximum of $U(\omega,\theta)$. The y axis is plotted on a linear scale in (a),(c) but on a log scale in (b),(d). (e)–(h) Distribution of the excited magnetic field H^r_ϕ, where each green line represents the BN slab. At the frequency of 24.5 THz, the relative permittivity of BN has $\varepsilon_\perp = 7.7 + 0.01i$ and $\varepsilon_z = -0.05 + 0.04i$.

Besides, the angular spectral feature of transition radiation at the frequency with $\varepsilon_z \to 0$ in Figs. 3(a) and 3(b) is entirely different from those at frequencies without $\varepsilon_z \to 0$ in Figs. 3(c) and 3(d). At the frequency without $\varepsilon_z \to 0$, $U(\omega,\theta)$ in Figs. 3(c) and 3(d) monotonically increases with v. Meanwhile, the maximum of $U(\omega,\theta)$ starts to appear at a relatively small radiation angle (<45°) if $v/c > 0.3$ in Figs. 3(c) and 3(d).

To confirm the unique angular feature above, Figs. 3(e) and 3(f) show the field distribution of the excited waves at the frequency with $\varepsilon_z \to 0$. Remarkably, the field strength with $v/c = 0.001$ in Fig. 3(f) is comparable to that with $v/c = 0.999$ in Fig. 3(e). However, the excited waves mainly propagate to the directions almost parallel to the interface (with $\theta \to 90°$) if $v/c = 0.001$ in Fig. 3(f), which is similar to the dipolar radiation induced by a dipole oscillating in a direction vertical to the epsilon-near-zero slab, while most of the excited waves would propagate to the direction almost perpendicularly to the interface (with $\theta \to 0°$) if $v/c = 0.999$ in Fig. 3(e). For comparison, we show the excited waves at the frequency without $\varepsilon_z \to 0$ [e.g., in Figs. 3(g) and 3(h), and in Fig. S6 [54]] By contrast, the field strength with $v/c = 0.001$ in Fig. 3(h) is much weaker than that with $v/c = 0.999$ in Fig. 3(g).

Since the low-velocity-favored transition radiation mainly occurs near the frequency with $\varepsilon_z \to 0$, its origin is closely related to the excitation of Ferrell-Berreman modes [4,40,41]. Essentially, the underlying mechanism for the transition radiation of Ferrell-Berreman modes is that the bulk plasmons provide a unique route to extend the electron-interface interaction time, then create light emission far beyond the conventional formation time historically defined for free-electron radiation, and thus help to greatly enhance the radiation intensity [4]. In other words, the emergence of a long tail of bulk plasmons following the electron's trajectory deep into the epsilon-near-zero material mixes surface and bulk effect, and it provides a sustained channel for electron-interface interaction [4]. In addition, the consideration of the nonlocal response of epsilon-near-zero materials and the excitation of longitudinal waves has a minor influence on the angular spectral energy density and the radiation spectrum of excited propagating waves [4]. On the other hand, the low-velocity-favored transition radiation can occur if a moving electron penetrates through an epsilon-near-zero slab in Figs. 2 and 3 but would not appear if the electron crosses a single interface between an epsilon-near-zero material and free space in Fig. S1, despite the excitation of Ferrell-Berreman modes in both scenarios. In this way, the revealed phenomenon of low-velocity-favored transition radiation, including the plateau and the dip in Fig. 2(b), could be ascribed to the interference between the excited Ferrell-Berreman modes, instead of merely the excitation of Ferrell-Berreman modes.

The Ferrell-Berreman mode itself has been extensively studied, including that in anisotropic systems [41,65–67]. The transition radiation of Ferrell-Berreman modes has also been extensively discussed but is focused on the isotropic materials (e.g., a metal slab) [4,40,46–49]. However, the study of transition radiation of Ferrell-Berreman modes in

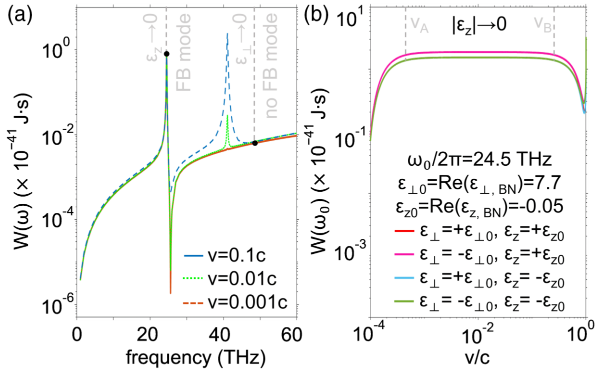

FIG. 4. Existence of the low-velocity-favored transition radiation in various epsilon-near-zero materials. (a) Radiation spectrum of transition radiation from a uniaxial BN slab with the consideration of material loss. The radiation peak near the frequency with $\varepsilon_z \to 0$ is related to the excitation of Ferrell-Berreman (FB) modes, while there is no radiation peak near the frequency with $\varepsilon_\perp \to 0$. (b) Radiation spectrum of transition radiation from uniaxial materials with $|\varepsilon_z| \to 0$; the structural setup is the same as Fig. 2(a), except for the permittivity of region 2. For conceptual illustration, the material loss is neglected in (b).

other complex anisotropic systems, including uniaxial materials (e.g., BN), has been relatively less explored. For uniaxial materials, $\varepsilon_z \to 0$ and $\varepsilon_\perp \to 0$ are in principle both possible. It is then natural to ask whether $\varepsilon_z \to 0$ or $\varepsilon_\perp \to 0$ is the crucial parameter to create the low-velocity-favored transition radiation.

To address this issue, Fig. 4(a) replots the radiation spectrum of transition radiation from BN in Fig. 2(a) under three fixed velocities. For BN, we have $\varepsilon_\perp \to 0$ near 48.2 THz (namely $\varepsilon_\perp = 0.02 + 0.08i$ and $\varepsilon_z = 2.8 + 0.0003i$), in addition to $\varepsilon_z \to 0$ near 24.5 THz. A radiation peak, which is a characteristic signature of the Ferrell-Berreman mode, always shows up near 24.5 THz but does not emerge near 48.2 THz in Fig. 4(a). Hence, $\varepsilon_z \to 0$, instead of $\varepsilon_\perp \to 0$, plays a crucial role in the excitation of Ferrell-Berreman modes. Moreover, Fig. 4(b) shows the transition radiation from various uniaxial epsilon-near-zero materials with $|\varepsilon_z| \to 0$, where the material loss is neglected and the other structural setup is the same as that in Fig. 2(a). The phenomenon of the low-velocity-favored transition radiation always appears, no matter $\mathrm{Re}(\varepsilon_z) > 0$ or $\mathrm{Re}(\varepsilon_z) < 0$. Meanwhile, the appearance of this phenomenon is relatively insensitive to the values of $\varepsilon_\perp$ in Fig. 4(b). Figure 4(b) also indicates that the occurrence of low-velocity-favored transition radiation does not necessarily require the existence of high-k modes in epsilon-near-zero materials (Fig. S5 [54]), since it is not caused by Cherenkov radiation of high-k modes (Fig. S9) (e.g., that inside a hyperbolic material [28–32]). From Figs. 4(a) and 4(b), we then conclude that $|\varepsilon_z| \to 0$ plays a determinant role in the creation of the low-velocity-favored transition radiation. Therefore, it is better to exploit $|\varepsilon_z| \to 0$, instead of $|\varepsilon_\perp| \to 0$, for the design of novel light sources based on low-energy electrons.

In conclusion, we have demonstrated a feasible route to achieve the low-velocity-favored transition radiation by exploiting the Ferrell-Berreman mode in epsilon-near-zero materials. Such an exotic phenomenon of free-electron radiation can simultaneously achieve strong emission intensity and high photon extraction efficiency readily from low-energy electrons. Because of the abundance of epsilon-near-zero materials in nature or through judicious nanofabrication [68–73], our finding of low-velocity-favored transition radiation can apply to a broad range of frequencies, e.g., microwave, terahertz, midinfrared, visible, and ultraviolet. Therefore, our finding not only enriches the physics of free-electron radiation but also broadens potential applications of Ferrell-Berreman modes, especially for the design of integrated free-electron light sources that are highly efficient and tunable.

X. L. acknowledges the support partly from the National Natural Science Fund for Excellent Young Scientists Fund Program (Overseas) of China, the National Natural Science Foundation of China under Grant No. 62175212, Zhejiang Provincial Natural Science Fund Key Project under Grant No. LZ23F050003, and the Fundamental Research Funds for the Central Universities (2021FZZX001-19). H. C. acknowledges the support from the Key Research and Development Program of the Ministry of Science and Technology under Grants No. 2022YFA1404704, No. 2022YFA1404902, and No. 2022YFA1405200, the National Natural Science Foundation of China under Grants No. 11961141010 and No. 61975176. J. C. acknowledges the support from the Chinese Scholarship Council (CSC No. 202206320287). I. K. acknowledges the support from the Israel Science Foundation under Grant No. 3334/19 and the Israel Science Foundation under Grant No. 830/19. Y. Y. acknowledges the support from the start-up fund of the University of Hong Kong and the National Natural Science Foundation of China Excellent Young Scientists Fund (HKU 12222417). B. Z. acknowledges the support from Singapore National Research Foundation Competitive Research Program No. NRF-CRP23-2019-0007.

[*]Corresponding author: kaminer@technion.ac.il
[†]Corresponding author: hansomchen@zju.edu.cn
[‡]Corresponding author: xiaolinzju@zju.edu.cn

[1] V. L. Ginzburg and I. M. Frank, Radiation of a uniformly moving electron due to its transition from one medium into another, Zh. Eksp. Teor. Fiz. **16**, 15 (1946).

[2] X. Lin, S. Easo, Y. Shen, H. Chen, B. Zhang, J. D. Joannopoulos, M. Soljačić, and I. Kaminer, Controlling Cherenkov angles with resonance transition radiation, Nat. Phys. **14**, 816 (2018).

[3] X. Lin, I. Kaminer, X. Shi, F. Gao, Z. Yang, Z. Gao, H. Buljan, J. D. Joannopoulos, M. Soljačić, H. Chen, and B. Zhang, Splashing transients of 2D plasmons launched by swift electrons, Sci. Adv. **3**, e1601192 (2017).

[4] F. Tay, X. Lin, X. Shi, H. Chen, I. Kaminer, and B. Zhang, Bulk-plasmon-mediated free-electron radiation beyond the conventional formation time, Adv. Sci. **10**, 2300760 (2023).

[5] J. Chen, H. Chen, and X. Lin, Photonic and plasmonic transition radiation from grapheme, J. Opt. **23**, 034001 (2020).

[6] F. J. García de Abajo, Optical excitations in electron microscopy, Rev. Mod. Phys. **82**, 209 (2010).

[7] C. Carmes, S. Kooi, Y. Yang, N. Rivera, P. Keathley, J. Joannopoulos, S. Johnson, I. Kaminer, K. Berggren, and M. Soljačić, Free-electron-light interactions in nanophotonics, Appl. Phys. Rev. **10**, 011303 (2023).

[8] S. Galyamin, A. Tyukhtin, A. Kanaeykin, and P. Schoessow, Reversed Cherenkov-Transition Radiation by a Charge Crossing a Left-Handed Medium Boundary, Phys. Rev. Lett. **103**, 194802 (2009).

[9] J. D. Jackson, *Classical Electrodynamics* (John Wiley & Sons, New York, 1999).

[10] M. Aguilar *et al.* (AMS Collaboration), Towards Understanding the Origin of Cosmic-Ray Positrons, Phys. Rev. Lett. **122**, 041102 (2019).

[11] X. Huang and K. Tuchin, Transition Radiation as a Probe of the Chiral Anomaly, Phys. Rev. Lett. **121**, 182301 (2018).

[12] K. D. Vries and S. Prohira, Coherent Transition Radiation from the Geomagnetically Induced Current in Cosmic-Ray Air Showers: Implications for the Anomalous Events Observed by ANITA, Phys. Rev. Lett. **123**, 091102 (2019).

[13] C. Carmes, N. Rivera, A. Ghorashi, S. E. Kooi, Y. Yang, Z. Lin, J. Beroz, A. Massuda, J. Sloan, N. Romeo, Y. Yu, J. D. Joannopoulos, I. Kaminer, S. G. Johnson, and M. Soljačić, A framework for scintillation in nanophotonics, Science **375**, 9293 (2022).

[14] D. Zhang, Y. Zeng, Y. Bai, Z. Li, Y. Tian, and R. Li, Coherent surface plasmon polariton amplification via free-electron pumping, Nature (London) **611**, 55 (2022).

[15] G. Q. Liao, Y. T. Li, Y. H. Zhang, H. Liu, X. L. Ge, S. Yang, W. Q. Wei, X. H. Yuan, Y. Q. Deng, B. J. Zhu, Z. Zhang, W. M. Wang, Z. M. Sheng, L. M. Chen, X. Lu, J. L. Ma, X. Wang, and J. Zhang, Demonstration of Coherent Terahertz Transition Radiation from Relativistic Laser-Solid Interactions, Phys. Rev. Lett. **116**, 205003 (2016).

[16] J. Déchard, A. Debayle, X. Davoine, L. Gremillet, and L. Bergé, Terahertz Pulse Generation in Underdense Relativistic Plasmas: From Photoionization-Induced Radiation to Coherent Transition Radiation, Phys. Rev. Lett. **120**, 144801 (2018).

[17] X. Xu, D. B. Cesar, S. Corde, V. Yakimenko, M. J. Hogan, C. Joshi, A. Marinelli, and W. B. Mori, Generation of Terawatt Attosecond Pulses from Relativistic Transition Radiation, Phys. Rev. Lett. **126**, 094801 (2021).

[18] M. Shentcis, A. Budniak, X. Shi, R. Dahan, Y. Kurman, M. Kalina, H. Sheinfux, M. Blei, M. Svendsen, Y. Amouyal, S. Tongay, K. Thygesen, F. H. L. Koppens, E. Lifshitz, F. J. G. Abajo, L. Wong, and I. Kaminer, Tunable free-electron x-ray radiation from van der Waals materials, Nat. Photonics **14**, 686 (2020).

[19] L. Wong, I. Kaminer, O. Ilic, J. D. Joannopoulos, and M. Soljačić, Towards graphene plasmon-based free-electron infrared to x-ray sources, Nat. Photonics **10**, 46 (2016).

[20] R. Chen, J. Chen, Z. Gong, X. Zhang, X. Zhu, Y. Yang, I. Kaminer, H. Chen, B. Zhang, and X. Lin, Free-electron Brewster-transition radiation, Sci. Adv. **9**, adh8098 (2023); see also arXiv:2302.09495.

[21] R. Chen, Z. Gong, J. Chen, X. Zhang, X. Zhu, H. Chen, and X. Lin, Recent advances of transition radiation: Fundamentals and applications, Mater. Today Electron. **3**, 100025 (2023).

[22] Y. Adiv, H. Hu, S. Tsesses, R. Dahan, K. Wang, Y. Kurman, A. Gorlach, H. Chen, X. Lin, G. Bartal, and I. Kaminer, Observation of 2D Cherenkov Radiation, Phys. Rev. X **13**, 011002 (2023).

[23] Z. Duan, X. Tang, Z. Wang, Y. Zhang, X. Chen, M. Chen, and Y. Gong, Observation of the reversed Cherenkov radiation, Nat. Commun. **8**, 14901 (2017).

[24] A. Polman, M. Kociak, and F. J. García de Abajo, Electron-beam spectroscopy for nanophotonics, Nat. Mater. **18**, 1158 (2019).

[25] H. Hu, X. Lin, and Y. Luo, Free-electron radiation engineering via structured environments, Prog. Electromagn. Res. **171**, 75 (2021).

[26] Z. Su, B. Xiong, Y. Xu, Z. Cai, J. Yin, R. Peng, and Y. Liu, Manipulating Cherenkov radiation and Smith-Purcell radiation by artificial structures, Adv. Opt. Mater. **7**, 1801666 (2019).

[27] G. Huang, N. J. Engelsen, O. Kfir, C. Ropers, and T. J. Kippenberg, Coupling ideality of free electrons with photonic integrated waveguides, PRX Quantum **4**, 020351 (2023).

[28] H. Hu, X. Lin, J. Zhang, D. Liu, P. Genevet, B. Zhang, and Y. Luo, Nonlocality induced Cherenkov threshold, Laser Photonics Rev. **14**, 2000149 (2020).

[29] F. Liu, L. Xiao, Y. Ye, M. Wang, K. Cui, X. Feng, W. Zhang, and Y. Huang, Integrated Cherenkov radiation emitter eliminating the electron velocity threshold, Nat. Photonics **11**, 289 (2017).

[30] X. Guo, C. Wu, S. Zhang, D. Hu, S. Zhang, Q. Jiang, X. Dai, Y. Duan, X. Yang, Z. Sun, S. Zhang, H. Xu, and Q. Dai, Mid-infrared analogue polaritonic reversed Cherenkov radiation in natural anisotropic crystals, Nat. Commun. **14**, 2532 (2023).

[31] J. Tao, L. Wu, G. Zheng, and S. Yu, Cherenkov polaritonic radiation in a natural hyperbolic material, Carbon **150**, 136 (2019).

[32] X. Zhang, M. Hu, Z. Zhang, Y. Wang, T. Zhang, X. Xu, T. Zhao, Z. Wu, R. Zhong, D. Liu, Y. Wei, Y. Gong, and S. Liu, High-efficiency threshold-less Cherenkov radiation generation by a graphene hyperbolic grating in the terahertz band, Carbon **183**, 225 (2021).

[33] X. Lin, H. Hu, S. Easo, Y. Yang, Y. Shen, K. Yin, M. P. Blago, I. Kaminer, B. Zhang, H. Chen, J. Joannopoulos, M. Soljačić, and Y. Luo, A Brewster route to Cherenkov detectors, Nat. Commun. **12**, 5554 (2021).

[34] S. Liu, P. Zhang, W. Liu, S. Gong, R. Zhong, Y. Zhang, and M. Hu, Surface Polariton Cherenkov Light Radiation Source, Phys. Rev. Lett. **109**, 153902 (2012).

[35] J. Henke, A. Raja, A. Feist, G. Huang, G. Arend, Y. Yang, F. Kappert, R. Wang, M. Möller, J. Pan, J. Liu, O. Kfir, C. Ropers, and T. Kippenberg, Integrated photonics enables

continuous-beam electron phase modulation, Nature (London) **600**, 653 (2021).

[36] S. Kwon, R. Ota, E. Berg, F. Hashimoto, K. Nakajima, I. Ogawa, Y. Tamagawa, T. Omura, T. Hasegawa, and S. R. Cherry, Ultrafast timing enables reconstruction-free positron emission imaging, Nat. Photonics **15**, 914 (2021).

[37] H. Hu, X. Lin, D. Liu, H. Chen, B. Zhang, and Y. Luo, Broadband enhancement of Cherenkov radiation using dispersionless plasmons, Adv. Sci. **9**, 2200538 (2022).

[38] N. Kotagiri, G. Sudlow, W. Akers, and S. Achilefu, Breaking the depth dependency of phototherapy with Cerenkov radiation and low-radiance-responsive nanophotosensitizers, Nat. Nanotechnol. **10**, 370 (2015).

[39] H. Hu, X. Lin, L. J. Wong, Q. Yang, D. Liu, B. Zhang, and Y. Luo, Surface Dyakonov-Cherenkov radiation, eLight **2**, 2 (2022).

[40] R. A. Ferrell, Predicted radiation of plasma oscillations in metal films, Phys. Rev. **111**, 1214 (1958).

[41] D. W. Berreman, Infrared absorption at longitudinal optic frequency in cubic crystal films, Phys. Rev. **130**, 2193 (1963).

[42] W. D. Newman, C. L. Cortes, J. Atkinson, S. Pramanik, R. G. DeCorby, and Z. Jacob, Ferrell-Berreman modes in plasmonic epsilon-near-zero media, ACS Photonics **2**, 2 (2015).

[43] A. Kubo, K. Onda, H. Petek, Z. Sun, Y. Jung, and H. K. Kim, Femtosecond imaging of surface plasmon dynamics in a nanostructured silver film, Nano Lett. **5**, 1123 (2006).

[44] N. Liu, T. Weiss, M. Mesch, L. Langguth, U. Eigenthaler, M. Hirscher, C. Sonnichsen, and H. Giessen, Planar metamaterial analogue of electromagnetically induced transparency for plasmonic sensing, Nano Lett. **10**, 1103 (2009).

[45] W. Jia, M. Liu, Y. Lu, X. Feng, Q. Wang, X. Zhang, Y. Ni, F. Hu, M. Gong, X. Xu, Y. Huang, W. Zhang, Y. Yang, and J. Han, Broadband terahertz wave generation from an epsilon-near-zero material, Light Sci. Appl. **10**, 11 (2021).

[46] E. A. Stern, Transition Radiation from Metal Films, Phys. Rev. Lett. **8**, 7 (1962).

[47] E. T. Arakawa, N. O. Davis, and R. D. Birkhoff, Temperature and thickness dependence of transition radiation from thin silver foils, Phys. Rev. **135**, A224 (1964).

[48] N. Yamamoto, H. Sugiyama, and A. Toda, Cherenkov and transition radiation from thin plate crystals detected in the transmission electron microscope, Proc. R. Soc. A **452**, 2279 (1996).

[49] F. J. García de Abajo and M. Kociak, Probing the Photonic Local Density of States with Electron Energy Loss Spectroscopy, Phys. Rev. Lett. **100**, 106804 (2008).

[50] Y. Yang, A. Massuda, C. R. Carmes, S. E. Kooi, T. Christensen, S. G. Johnson, J. D. Joannopoulos, O. D. Miller, I. Kaminer, and M. Soljačić, Maximal spontaneous photon emission and energy loss from free electrons, Nat. Phys. **14**, 894 (2018).

[51] H. Liu, N. J. Outmezguine, D. Redigolo, and T. Volansky, Reviving millicharged dark matter for 21-cm cosmology, Phys. Rev. D **100**, 123011 (2019).

[52] Y. Hochberg, Y. Kahn, N. Kurinsky, B. V. Lehmann, T. C. Yu, and K. K. Berggren, Determining Dark-Matter-Electron Scattering Rates from the Dielectric Function, Phys. Rev. Lett. **127**, 151802 (2021).

[53] A. Berlin and K. Schutz, Helioscope for gravitationally bound millicharged particles, Phys. Rev. D **105**, 095012 (2022).

[54] See Supplemental Material at http://link.aps.org/supplemental/10.1103/PhysRevLett.131.113002 for detailed derivations and discussions.

[55] S. Dai, Z. Fei, Q. Ma, A. S. Rodin, M. Wagner, A. S. McLeod, M. K. Liu, W. Gannett, W. Regan, K. Watanabe, T. Taniguchi, M. Thiemens, G. Dominguez, A. H. Castro Neto, A. Zettl, F. Keilmann, P. Jarillo-Herrero, M. M. Fogler, and D. N. Basov, Tunable phonon polaritons in atomically thin van der Waals crystals of boron nitride, Science **343**, 1125 (2014).

[56] J. D. Caldwell, I. Aharonovich, G. Cassabois, J. H. Edgar, B. Gil, and D. N. Basov, Photonics with hexagonal boron nitride, Nat. Rev. Mater. **4**, 552 (2019).

[57] N. Rivera, T. Christensen, and P. Narang, Phonon polaritonics in two-dimensional materials, Nano Lett. **19**, 2653 (2019).

[58] X. Lin, Y. Yang, N. Rivera, J. J. López, Y. Shen, I. Kaminer, H. Chen, B. Zhang, J. D. Joannopoulos, and M. Soljačić, All-angle negative refraction of highly squeezed plasmon and phonon polaritons in graphene-boron nitride heterostructures, Proc. Natl. Acad. Sci. U.S.A. **114**, 6717 (2017).

[59] S. Roy, X. Zhang, A. Puthirath, A. Meiyazhagan, S. Bhattacharyya, M. Rahman, G. Babu, S. Susarla, S. Saju, M. Tran *et al.*, Structure, properties and applications of two-dimensional hexagonal boron nitride, Adv. Mater. **33**, 2101589 (2021).

[60] T. Low, A. Chaves, J. D. Caldwell, A. Kumar, N. X Fang, P. Avouris, T. F. Heinz, F. Guinea, L. M. Moreno, and F. Koppens, Polaritons in layered two-dimensional materials, Nat. Mater. **16**, 182 (2017).

[61] M. Turunen, M. B. Gisbert, Y. Dai, Y. Wang, E. Scerri, C. Bonato, K. D. Jöns, Z. Sun, and B. D. Gerardot, Quantum photonics with layered 2D materials, Nat. Rev. Phys. **4**, 219 (2022).

[62] X. Lin, R. Li, F. Gao, E. Li, X. Zhang, B. Zhang, and H. Chen, Loss induced amplification of graphene plasmons, Opt. Lett. **41**, 681 (2016).

[63] Y. Jiang, X. Lin, T. Low, B. Zhang, and H. Chen, Group-velocity-controlled and gate-tunable directional excitation of polaritons in graphene-boron nitride heterostructures, Laser Photonics Rev. **12**, 1800049 (2018).

[64] W. Chew, *Waves and Fields in Inhomogeneous Media* (IEEE Press, New York, 1994).

[65] S. Vassant, J. Hugonin, F. Marquier, and J. Greffet, Berreman mode and epsilon near zero mode, Opt. Express **20**, 23971 (2012).

[66] D. Pratap, J. Pradhan, and S. Ramakrishna, Experimental observation of Berreman modes in an uniaxial anisotropic nanoporous alumina film on aluminum substrate, Opt. Lett. **47**, 2554 (2022).

[67] W. Newman, C. Cortes, J. Atkinson, S. Pramanik, R. DeCorby, and Z. Jacob, Ferrell-Berreman modes in plasmonic epsilon-near-zero media, ACS Photonics **2**, 2 (2015).

[68] E. Vesseur, T. Coenen, H. Caglayan, N. Engheta, and A. Polman, Experimental Verification of $n = 0$ Structures for Visible Light, Phys. Rev. Lett. **110**, 013902 (2013).

[69] N. Kinsey, C. DeVault, A. Boltasseva, and V. M. Shalaev, Near-zero-index materials for photonics, Nat. Rev. Mater. **4**, 742 (2019).

[70] O. Reshef, I. D. Leon, M. Z. Alam, and R. W. Boyd, Nonlinear optical effects in epsilon-near-zero media, Nat. Rev. Mater. **4**, 535 (2019).

[71] J. Wu, Z. Xie, Y. Sha, H. Y. Fu, and Q. Li, Epsilon-near-zero photonics: Infinite potentials, Photonics Res. **9**, 1616 (2021).

[72] C. Wang, C. Qian, H. Hu, L. Shen, Z. Wang, H. Wang, Z. Xu, B. Zhang, H. Chen, and X. Lin, Superscattering of light in refractive-index near-zero environments, Prog. Electromagn. Res. **168**, 15 (2020).

[73] J. Chen, X. Lin, M. Chen, T. Low, H. Chen, and S. Dai, A perspective of twisted photonic structures, Appl. Phys. Lett. **119**, 240501 (2021).